Computer Physics Communications 129 (2000) 110–120

Computer Physics Communications

www.elsevier.nl/locate/cpc

Application of lattice Boltzmann model to multiphase flows with phase transition

Koji Kono [a,*], Tatsumi Ishizuka [a], Hiroshi Tsuda [b], Atsushi Kurosawa [b]

[a] *Fuji Research Institute Corporation, Takebashi Square, 2-3 Kandanishiki-cho, Chiyoda-ku, Tokyo 101-8443, Japan*
[b] *The Institute of Applied Energy, 14-2 Nishishinbashi 1-chome, Minato-ku, Tokyo 105-0003, Japan*

Abstract

A lattice Boltzmann model for multiphase flows is extended to simulate multi-phase fluids flows with phase transition by taking an account of mass exchange process in the lattice Boltzmann equation. The numerical measurements in terms of bulk properties such as volume fraction and density agree with analytical solutions of mass and volume conservation through simulations of phase transitions with homogeneous transition rate. The simulations of phase transition under gravity including pool boiling and boiling flow in a vertical pipe demonstrate qualitative applicability of the model to simulation of complicated multi-phase fluid dynamics with phase transition.

PACS: 47.55.K

Keywords: Multi-phase flow; Phase transition; Lattice Boltzmann method; Flow pattern change

1. Introduction

A numerical simulation of multi-phase fluid flows is an interesting and challenging problem owing to physical complexity and importance in many science and engineering related problems. In particular, a boiling two-phase flow is a highly complex nonlinear phenomenon including thermal hydraulics, phase transition, bubble and droplet dynamics coupled with interface interactions, so that the numerical solution of the equations describing the processes taking place in boiling two-phase flows is a highly laborious task.

Recently, several numerical approaches have been proposed for the multi-phase flow simulation focusing on individual bubble and droplet dynamics. The traditional approaches solve local instantaneous field equation of the gas–liquid flow by means of specific methods such as volume-of-fluid (VOF) [1], level-set method [2] and cubic-interpolated-pseudo-particle (CIP) [3]. An alternative approach is a numerical method based on microscopic kinetic equations for modeling multi-phase flow phenomena. In the last decade, the lattice gas computational fluid dynamics, including lattice gas automata (LGA) [4] and the lattice Boltzmann (LB) equation method [5] have attracted attentions in the application of multi-phase fluid flows (for reviews, see [6,7]). The lattice methods are based on discrete particle description of a fluid and provide many of the advantages of molecular dynamics such as clear physical pictures and allow us to define the complicated geometries. The lattice approaches have another

* Corresponding author. E-mail: kohno@star.fuji-ric.co.jp.

0010-4655/00/$ – see front matter
PII: S0010-4655(00)00098-9

advantage that parallel nature of these schemes affords an easy implementation of fast and efficient simulation on massively parallel computers.

The first LB model for solving two-component fluid flows by introducing an ideology of immiscible lattice gas (ILG) into the LB method was proposed by Gunstensen et al. [8]. Grunau et al. extended the LB model by including density and viscosity variations of fluid components [9]. Shan and Chen proposed a different LB model for multi-phase flow using "pseudo-potential" for non-trivial equations of state [10,11]. Swift et al. proposed a LB model with BGK collision for van der Waals equation of state by free energy argument [12]. Seta et al. also proposed another LBGK model [13] to reproduce fluid dynamic equation based on van der Waals–Cahn–Hilliard free energy. The model has been extended using multi-speed particle to consider thermal effects [14]. Though these models have a potential to reproduce multi-phase fluid flows, they have not been applied to practical phase change phenomena such as boiling flows.

In this paper, we extend the lattice Boltzmann model for multi-phase immiscible fluid flows proposed by Grunau et al. [9] by considering mass exchange process to simulate multi-phase flow dynamics with phase transition. The LB model provides reproduction of multi-phase fluid dynamics based on Navier–Stokes equation coupled with phase transition. The bulk properties calculated through simulations of phase transition with homogeneous transition rate agree with analytical solutions of mass and volume conservation. The simulations of phase transition under gravity demonstrates qualitative applicability of the model to simulation of highly complicated multi-phase fluid phenomena such as boiling flows. The proposed model is so preliminary because it does not consider thermal effects. The most realistic phase transitions are usually accompanied by heat evolution and absorption due to a latent heat of condensation or evaporation. The model might be improved by incorporating thermal effects by introducing thermal LBGK models into it.

2. A lattice Boltzmann model for multi-phase flows

The lattice Boltzmann model (LBM) for multi-phase fluid flows with phase transition starts from the following kinetic equation for the discrete velocity distribution function, f_i^k for red and blue fluids on a discrete lattice:

$$f_i^k\left(\boldsymbol{x}+\boldsymbol{e}_i^\sigma, t+1\right) = f_i^k(\boldsymbol{x},t) + \Omega_i^k(\boldsymbol{x},t) + G_i^k + \Gamma_i^k, \tag{1}$$

where k denotes colors of particles, red or blue, which are introduced to distinguish changeable phases. i and σ are the moving particle direction and magnitude of velocity, respectively. The total density distribution $f_i(\boldsymbol{x},t)$ is a sum of the red and blue fluid density distributions defined as $f_i(\boldsymbol{x},t) = f_i^r(\boldsymbol{x},t) + f_i^b(\boldsymbol{x},t)$. The $\Omega_i^k(\boldsymbol{x},t)$ is a collision operator and G_i^k is a external force reproducing gravity force. The Γ_i^k represents phase exchange process. The collision term, $\Omega_i^k(\boldsymbol{x},t)$ is comprised of two parts, $\Omega_i^k = (\Omega_i^k)^A + (\Omega_i^k)^B$. The first term, $(\Omega_i^k)^A$, represents a process of relaxation to local equilibrium. For the linearized collision operator with a single time relaxation parameter or the lattice BGK [5,17],

$$(\Omega_i^k)^A = -\frac{1}{\tau_k}\left(f_i^k - f_i^{k(0)}\right). \tag{2}$$

Here τ_k is the relaxation time for species k and $f_i^{k(0)}$ is the local equilibrium distribution function depending on the local density, velocity and the specific lattice used. The local equilibrium state can be arbitrarily chosen, with the exception that it satisfies the conservation of mass and momentum:

$$\rho_r = \sum_i f_i^r = \sum_i f_i^{r(\mathrm{eq})}, \qquad \rho_b = \sum_i f_i^b = \sum_i f_i^{b(\mathrm{eq})}$$

and

$$\rho\boldsymbol{v} = \sum_{i,k} f_i^k \boldsymbol{e}_i^\sigma = \sum_{i,k} f_i^{k(\mathrm{eq})} \boldsymbol{e}_i^\sigma.$$

Here ρ_r and ρ_b are densities of the red and blue fluids, respectively, $\rho = \rho_r + \rho_b$ is the total density, and $\boldsymbol{v}$ is the local velocity.

There are several lattice structures proposed for 2D and 3D LB models [4,18]. We choose 2D square lattice with rest particle [17] and assume the following equilibrium distribution for both red and blue fluids:

$$f_i^{k,\sigma(0)} = \rho_k\big(A_k^\sigma + B_k^\sigma(\boldsymbol{e}_i^\sigma \cdot \boldsymbol{v}) + C_k^\sigma(\boldsymbol{e}_i^\sigma \cdot \boldsymbol{v})^2 - D_k^\sigma v^2\big). \tag{3}$$

Here σ denote types of moving particles. Particles of type I move along the axes with speed $|\boldsymbol{e}_i^{\mathrm{I}}| = 1$ and particles of type II move along the diagonal directions with speed $|\boldsymbol{e}_i^{\mathrm{II}}| = \sqrt{2}$.

The second part of the collision operator is a same expression given by Grunau et al. [9],

$$(\Omega_i^k)^B = \frac{4}{3}A_k|\boldsymbol{F}|\left[\frac{(\boldsymbol{e}_i^\sigma \cdot \boldsymbol{F})^2}{|\boldsymbol{F}|^2} - \frac{3}{4}\right], \tag{4}$$

where $\boldsymbol{F}$ is the local color gradient, defined as

$$\boldsymbol{F} = \sum_i \boldsymbol{e}_i^\sigma\big[\rho_r(\boldsymbol{x} + \boldsymbol{e}_i^\sigma) - \rho_b(\boldsymbol{x} + \boldsymbol{e}_i^\sigma)\big].$$

Here A_k is a parameter controlling surface tension. $\boldsymbol{F}$ diminishes to zero in a single phase region so that the second term of the collision operator has influence at the vicinity of interfacial region. The redistribution of colored particles at the two-phase interfaces is performed to maintain surfaces by maximizing $-(\boldsymbol{j}^r \cdot \boldsymbol{F})$. Here $\boldsymbol{j}^r$ is a mass flux of red fluid, $\sum_i f_i^r \boldsymbol{e}_i^\sigma$.

The gravity force term, G_i^k is expressed as $G_i^k = \frac{\rho_k}{6}(\boldsymbol{e}_i^\sigma \cdot \boldsymbol{g})$, where $\boldsymbol{g}$ is a gravity force constant. This term does not contribute to mass conservation but contributes to momentum equation since $\sum_{k,i} G_i^k = 0$ and $\sum_{k,i} \boldsymbol{e}_i^\sigma G_i^k = \rho\boldsymbol{g}$.

Assuming isothermal condition, the phase change leads to combination of mass and momentum transports phenomenon. The phase change between red and blue fluids can be written as $B \rightleftharpoons R$, where the B and R represent "blue" phase and "red" phase, respectively. The phase change process is macroscopically expressed as

$$\frac{\partial\rho_r}{\partial t} = -\Theta_{r\to b}\rho_r + \Theta_{b\to r}\rho_b, \qquad \frac{\partial\rho_b}{\partial t} = -\Theta_{b\to r}\rho_b + \Theta_{r\to b}\rho_r. \tag{5}$$

Where $\Theta_{r\to b}$, $\Theta_{r\to b}$ are phase change rate from red phase to blue phase and from blue phase to red phase, respectively. In order to recover above phase exchange process, mesoscopic mass exchange term in the LB equation, Γ_i^k may have the following expression,

$$\Gamma_i^r = -\theta_{i,r\to b}f_i^r + \theta_{i,b\to r}f_i^b, \quad \text{and} \quad \Gamma_i^b = -\theta_{i,b\to r}f_i^b + \theta_{i,r\to b}f_i^r.$$

Here, $\theta_{i,r\to b}$, $\theta_{i,b\to r}$ are mesoscopic phase transition rates. This relation locally conserves total mass and momentum, namely, $\sum_{k,i}(\Gamma_i^r + \Gamma_i^b) = 0$, and $\sum_{k,i}\boldsymbol{e}_i^\sigma(\Gamma_i^r + \Gamma_i^b) = 0$. For simplicity, the mesoscopic phase transition rates are constant in each particle direction. This assumption leads to $\theta_{i,r\to b} = \Theta_{r\to b}$ and $\theta_{i,b\to r} = \Theta_{b\to r}$.

A long-wavelength, low-frequency approximation, the lattice spacing and the time increment of the LB equation can be regarded as small parameters of the same order, ϵ. Applying a Taylor expansion in time and space provides the following continuum expression of the kinetic equation accurate to second order in ϵ:

$$\begin{aligned}&\frac{\partial f_i^k}{\partial t} + \boldsymbol{e}_i^\sigma \cdot \nabla f_{ik} + \frac{1}{2}\boldsymbol{e}_i^\sigma\boldsymbol{e}_i^\sigma : \nabla\nabla f_{ik} + \boldsymbol{e}_i^\sigma \cdot \nabla\frac{\partial f_{ik}}{\partial t} + \frac{1}{2}\frac{\partial^2 f_i}{\partial t^2}\\ &\quad = (\Omega_i^k)^A + (\Omega_i^k)^B + G_i^k + \Gamma_i^k.\end{aligned} \tag{6}$$

For the derivation of hydrodynamic equations for multi-phase flows, we use a following Chapman–Enskog multi-scale expansion,

$$\frac{\partial}{\partial t} = \epsilon\frac{\partial}{\partial t_1} + \epsilon^2\frac{\partial}{\partial t_2} + \cdots, \quad \frac{\partial}{\partial x} = \epsilon\frac{\partial}{\partial x_1}.$$

The particle distribution function, f_i^k can be also expanded formally about the local equilibrium distribution function, $f_i^k = f_i^{k(0)} + \epsilon f_i^{k(1)} + \epsilon^2 f_i^{k(2)} + \cdots$.

Applying the multi-scale expansion to the Eq. (6) and taking the zeroth and first-order moments of $\boldsymbol{e}_i^\sigma$, we obtain the continuum equations for the red and blue fluids and the momentum equation for the total fluid. The recovered continuum equation is

$$\frac{\partial \rho}{\partial t} + \frac{\partial}{\partial x_\beta} \sum_{i,k} (\boldsymbol{e}_i^\sigma)_\beta f_i^{k(0)} = 0, \tag{7}$$

and the momentum equation is

$$\frac{\partial \rho u_\alpha}{\partial t} + \frac{\partial}{\partial x_\beta} \left[\Pi_{\alpha\beta}^0 + \left(1 - \frac{1}{2\hat{\tau}}\right) \Pi_{\alpha\beta}^1 \right] = -\frac{1}{2} \frac{\partial}{\partial x_\beta} \Lambda_{\alpha\beta}^0. \tag{8}$$

Here we define $\Pi_{\alpha\beta}^{(l)} = \sum_{i,k} (\boldsymbol{e}_i^\sigma)_\alpha (\boldsymbol{e}_i^\sigma)_\beta f_i^{k(l)}$, and $\Lambda_{\alpha\beta}^{(l)} = \sum_{i,k} (\boldsymbol{e}_i^\sigma)_\alpha (\boldsymbol{e}_i^\sigma)_\beta (\Omega_i^k)^{B(l)}$, respectively. Substituting the equilibrium distribution function, the momentum flux to ϵ order $\Pi_{\alpha\beta}^{(0)}$ satisfies $\Pi_{\alpha\beta}^{(0)} = (C_s)^2 \rho \delta_{\alpha\beta} + \rho u_\alpha u_\beta$. Here C_s is a sound speed. Applying the ϵ order equation, the contribution of higher order, $\Pi_{\alpha\beta}^{(1)}$ is rewritten as

$$\Pi_{\alpha\beta}^{(1)} = -\hat{\tau} \sum_{i,k} (\boldsymbol{e}_i^\sigma)_\alpha (\boldsymbol{e}_i^\sigma)_\beta \left(\frac{\partial f_i^{(0)}}{\partial t_1} + \boldsymbol{e}_i^\sigma \cdot \nabla f_i^{(0)} - (\Omega_i)^{B(0)} \right) = \Pi'^{(1)}_{\alpha\beta} + \hat{\tau} \Lambda_{\alpha\beta}^{(0)}. \tag{9}$$

Here $\Pi'^{(1)}_{\alpha\beta}$ is a fluid dynamic stress tensor and $\Lambda_{\alpha\beta}^{(0)}$ is a tensor providing surface tension:

$$\Lambda_{\alpha\beta}^{(0)} = \frac{4}{3} A |\boldsymbol{F}| \left[\frac{8 F_\alpha F_\beta - 6 F_\alpha F_\beta \delta_{\alpha\beta}}{|F|^2} - \frac{1}{2} \delta_{\alpha\beta} \right].$$

The momentum equation is finally written as

$$\begin{aligned} \frac{\partial}{\partial t} \rho u_\alpha + \frac{\partial}{\partial x_\beta} u_\alpha u_\beta = & -\frac{\partial}{\partial x_\beta} \left((C_s)^2 \rho \delta_{\alpha\beta} + \hat{\tau} \Lambda_{\alpha\beta}^{(0)} \right) \\ & + \left(\hat{\tau} - \frac{1}{2} \right) \left(\frac{1}{3} - (C_s)^2 \right) \frac{\partial}{\partial x_\alpha} \left(\frac{\partial}{\partial x_\gamma} \rho u_\gamma \right) \\ & + \left(\frac{2\hat{\tau} - 1}{6} \right) \frac{\partial}{\partial x_\beta} \rho \left(\frac{\partial}{\partial x_\alpha} u_\beta + \frac{\partial}{\partial x_\beta} u_\alpha \right) \\ & + \left(\hat{\tau} - \frac{1}{2} \right) \left(\frac{1}{3} - (C_s)^2 \right) \frac{\partial}{\partial x_\beta} \left(u_\beta \frac{\partial}{\partial x_\alpha} \rho + u_\alpha \frac{\partial}{\partial x_\beta} \rho \right) + \rho g_\alpha. \end{aligned} \tag{10}$$

The $\hat{\tau}$ is a relaxation parameter defined by a specific interpolation to deal with a smooth change of viscosity at the interfaces [9]. The shear viscosity ν is $(2\hat{\tau} - 1)/6$ and the sound speed is $\sqrt{6/(8 + m_k)}$. The surface tension effect included in Eq. (9) reproduces Laplace' law.

3. Phase transition with homogeneous transition rate

As the first application of the LB model to two-phase flows with phase transition, we carried out two basic numerical simulations of phase transition with homogeneous phase transition rate. In general, the phase transition phenomena have strong relation with thermodynamics and phase transition rate is a function of thermodynamic properties such as temperature and pressure. Unfortunately, since the proposed LB model does not consider energy conservation, applications of this LB model to phase change problems are limited to isothermal system, namely

isothermal saturated condition. Assuming that phases are saturated and isothermal, the heat exchange due to phase transition is regarded as the latent heat exchange. This assumption allows the macroscopic phase change rate to be written as $\Theta = \Delta q/\Delta h$, where Δq is heat flux supplied into the system and Δh is the latent heat of evaporation or condensation. The heat flux is a real-value input parameter in this model to control a speed of phase change phenomena. In our LB model, these phase transition phenomena are reproduced by follow processes.

(1) Intermediate state fluids are formed due to the mass exchange process, and then
(2) the unstable intermediate fluids become stable state of tiny vapor and liquid phases spontaneously by recoloring process.
(3) The tiny vapor or liquid phases merges and forms circular bubble or droplet as time evolves.

In a two-phase system used in the following simulations, a lower density of red fluid (corresponding to vapor phase) is 5.0 and a higher density of blue fluid (corresponding to liquid phase) is 10.0 under standard conditions. The density ratio γ between phases is 0.5. This value is much smaller comparing with actual two-phase system such as water liquid-vapor system. We use the phase change rate $\Theta_{b\to r} = \Delta q/\Delta h$ for $\Delta q \geqslant 0$ and $\Theta_{b\to r} = 0$ for $\Delta q < 0$ in the vaporization simulation and $\Theta_{r\to b} = 0$ for $\Delta q \geqslant 0$ and $\Theta_{r\to b} = \Delta q/\Delta h$ for $\Delta q < 0$ in the condensation simulation. Δh is assumed unity for simplicity.

The simulations imitate a vaporization (higher density phase changes to lower density phase) and a condensation (lower density phase changes to higher density phase) due to homogeneous heating or cooling in space and time. The whole domain is filled with blue liquid fluid which initial density ρ_b is 10.0 or red vapor fluid which initial density ρ_r is 5.0, respectively. The heat flux, Δq, supplied into and removed from the system are 0.002, and -0.002, respectively. Some perturbation is added into the heat flux. The simulation is carried out using lattice points, 128×128 and all boundaries are periodic. The relaxation parameter is 1.0 for blue liquid and red vapor fluid. The surface tension parameter is 0.001.

Figs. 1(a) and (b) show phase distributions of vaporization and condensation simulation at 200 step (lattice unit). The black color corresponds to lower density, red fluid and the gray color corresponds to higher density blue fluid. The size of vapor bubbles is bigger comparing with liquid droplets due to the density difference.

The solutions of macroscopic bulk properties for vaporization and condensation simulation can be analytically obtained by solving following equations:

$$\frac{\partial \rho_b V_b}{\partial t} = -\Theta_{b\to r}\rho_b V_b + \Theta_{r\to b}\rho_r V_r, \qquad \frac{\partial \rho_r V_r}{\partial t} = \Theta_{b\to r}\rho_b V_b - \Theta_{r\to b}\rho_r V_r, \tag{11}$$

where V_b and V_r are volume fractions of blue and red phase and satisfy $V_b + V_r = 1$. The densities of red and blue satisfy the ratio, $\gamma = 0.5$. The volume fractions of vapor, void fraction in vaporization ($V_{r,v}$) and condensation ($V_{r,c}$) simulation are

$$V_{r,v} = \frac{1 - \mathrm{e}^{-\Theta_{b\to r}t}}{1 + (\gamma - 1)\mathrm{e}^{-\Theta_{b\to r}t}}, \qquad V_{r,c} = \frac{\mathrm{e}^{-\Theta_{r\to b}t}}{\gamma + (1-\gamma)\mathrm{e}^{-\Theta_{r\to b}t}}. \tag{12}$$

The densities of liquid and vapor in vaporization, $\rho_{b,v}$, $\rho_{r,v}$ are

$$\rho_{b,v} = \frac{\rho_{b0}}{\gamma}\big(1 + (\gamma - 1)\mathrm{e}^{-\Theta_{b\to r}t}\big), \qquad \rho_{r,v} = \rho_{b0}\big(1 + (\gamma - 1)\mathrm{e}^{-\Theta_{b\to r}t}\big), \tag{13}$$

and the densities of liquid and vapor in condensation, $\rho_{b,c}$, $\rho_{r,c}$ are

$$\rho_{b,c} = \frac{\rho_{r0}}{\gamma}\big(\gamma + (1-\gamma)\mathrm{e}^{-\Theta_{r\to b}t}\big), \qquad \rho_{r,c} = \rho_{r0}\big(\gamma + (1-\gamma)\mathrm{e}^{-\Theta_{r\to b}t}\big), \tag{14}$$

where ρ_{b0} and ρ_{r0} are the initial densities of liquid and vapor, respectively. Fig. 2(a) shows time histories of volume fractions of vapor phase in vaporization and condensation simulations and Fig. 2(b) shows time histories of vapor and liquid densities in vaporization and condensation simulation, respectively. The bulk properties obtained by averaging numerical results agree well with analytical solutions except initial regions. This difference occurs due to a reason that the phases are not completely separated at initial regions in the simulations.

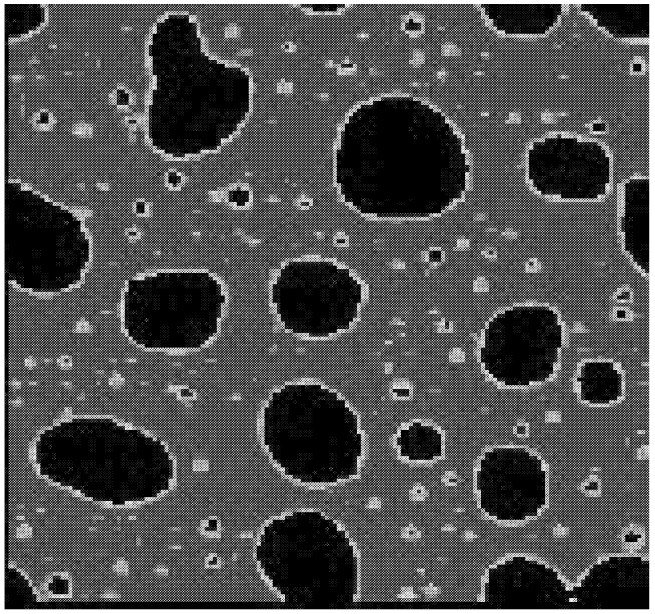

(a)

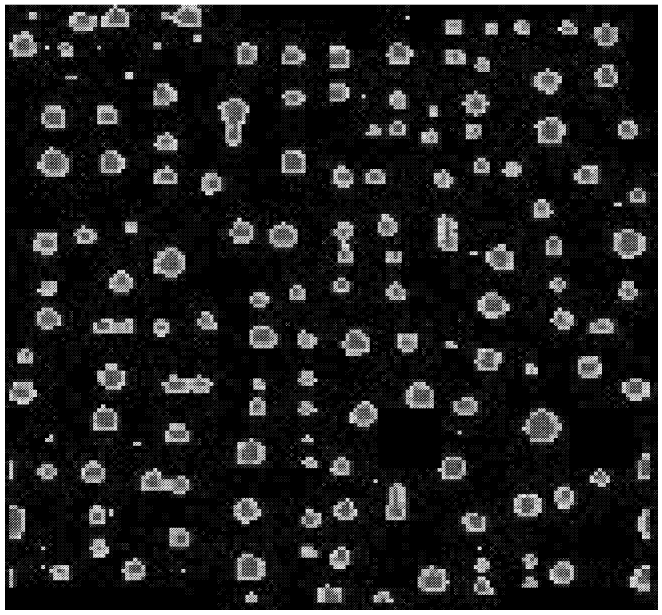

(b)

Fig. 1. Density distribution of phase transition simulation at time = 200. The black color corresponds to vapor of lower density and gray color corresponds to liquid of higher density. Figures (a) and (b) correspond to vaporization and condensation, respectively.

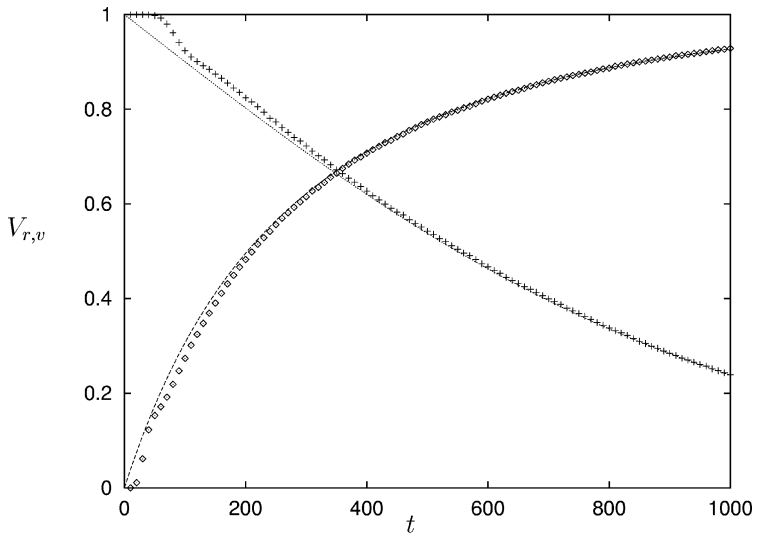

(a)

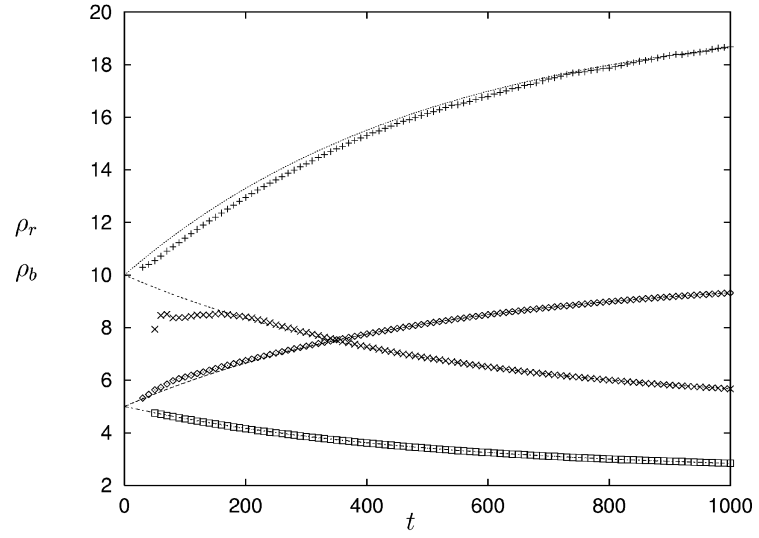

(b)

Fig. 2. (a) Time history of volume fraction of vapor phase (void fraction) for the vaporization ($\diamond$) and condensation ($+$) simulation. The dashed lines are analytical solutions given in the Eq. (12). (b) Time history of densities of vapor and liquid phase for the vaporization ($\diamond$, $+$) and condensation ($\square$, $\times$). The dashed lines are analytical solutions given in Eqs. (13) and (14).

4. Multi-phase flow simulation with phase change under gravity

In order to demonstrate applicability of the proposed LB model to practical multi-phase fluid flows with phase transition, simulations of two-phase flows with phase transition under gravity are carried out. The simulations imitate a pool boiling process and boiling flow in a vertical pipe by assuming the phase change process occurs only at a wall boundary.

4.1. Pool boiling

The pool boiling process is one of the most well-known phenomenon in two-phase flow dynamics coupled with phase transition. Pool boiling is a situation where boiling takes place by heating bottom wall in a stagnant pool of liquid. During boiling, natural and pumping convection play an important role in heat transfer mechanisms so that a prediction of flow properties is quite important for engineering propose such as boiling water reactor operations. Since the proposed LB model involves two-phase dynamics including surface tension, buoyancy due to gravity and phase change, it may reproduce pool boiling phenomena qualitatively despite the lack of energy conservation.

The phenomenological simulations of pool boiling process are carried out with following conditions. The simulations are performed using the lattice points, 200×200. The boundary conditions for right and left boundaries are periodic and standard bounce-back boundary is applied to a top wall. For the bottom wall, bounce-back boundary considering the phase change process is applied. The relaxation parameter is 1.0 for both fluids (liquid and vapor). The surface tension parameter is 0.002 and gravity force constant g_y is 0.0005. The stagnant pool is initially filled with liquid phase which density, ρ_b, is 10.0. The phase change occurs only at the bottom wall by a heat flux, Δh, i.e phase change rates, $\Theta_{b\to r}$, 0.01. Small perturbation is added into the heat flux.

The phase distributions at different time, 1000, 2000, 3000, and 4000 (lattice unit) are shown in Figs. 3(a), (b), (c) and (d), respectively. Small and spherical bubbles grow near the bottom wall and rise due to buoyancy. Collisions and coalescences occasionally happen while the bubbles rise. The result looks like a realistic nucleate boiling process in pool boiling. The reproduced phenomenon is not actual boiling process in the sense that energy conservation is not considered, however the proposed LB model demonstrates possibility of reproduction of boiling process with complicated fluid dynamics.

4.2. Boiling flow in a vertical pipe

The boiling flow phenomenon in a vertical pipe is more practical and typical in engineering systems such as boiling water reactors. One of the most interesting thing in the boiling flow in a vertical pipe is that a flow pattern changes from liquid phase flow to bubbly flow, plug flow, annular flow, mist flow and vapor flow. This flow pattern change occurs due to combination of phase transition caused heating from the wall and two-phase flow dynamics including bubble deformation, collision and coalescence.

The simulations boiling flow in a vertical pipe is carried out using the lattice points, 100×800. The boundary conditions for top and bottom boundaries are periodic and standard bounce-back boundary considering the phase change process is applied to side walls. The relaxation parameter is 1.0 for both fluid (liquid and vapor). The surface tension parameter is 0.001 and gravity force constant g_y is 0.0005. The vertical pipe is initially filled with liquid phase which density, ρ_b, is 10.0. The phase change occurs only at the side bottom wall by a constant heat flux, Δh, i.e. phase change rates, $\Theta_{b\to r}$, 0.001 with small perturbation.

The phase distributions at different time, 100, 1000, 2000, 4000, 6000, and 10 000 (lattice unit) are shown in Figs. 4(a), (b), (c), (d), (e) and (f), respectively. At an early stage of simulation (Fig. 4(a)), small vapor bubbles are created near the heated walls and rise up with deformation (Figs. 4(b) and (c)). As time evolves, size of bubbles becomes bigger due to collision and coalescence (Figs. 4(d) and (e)). At the end of simulation, the bubbles have ellipsoidal and plug shapes. This simulation reproduces a flow pattern change from liquid phase flow to bubbly flow, plug flow transitionally.

5. Conclusion

In this paper, we proposed a lattice Boltzmann model for multi-phase fluid flows coupled with phase transition by taking an account of mass exchange process in the lattice Boltzmann equation. The numerical measurements of bulk properties through vaporization and condensation simulation agree well with analytical solutions of density

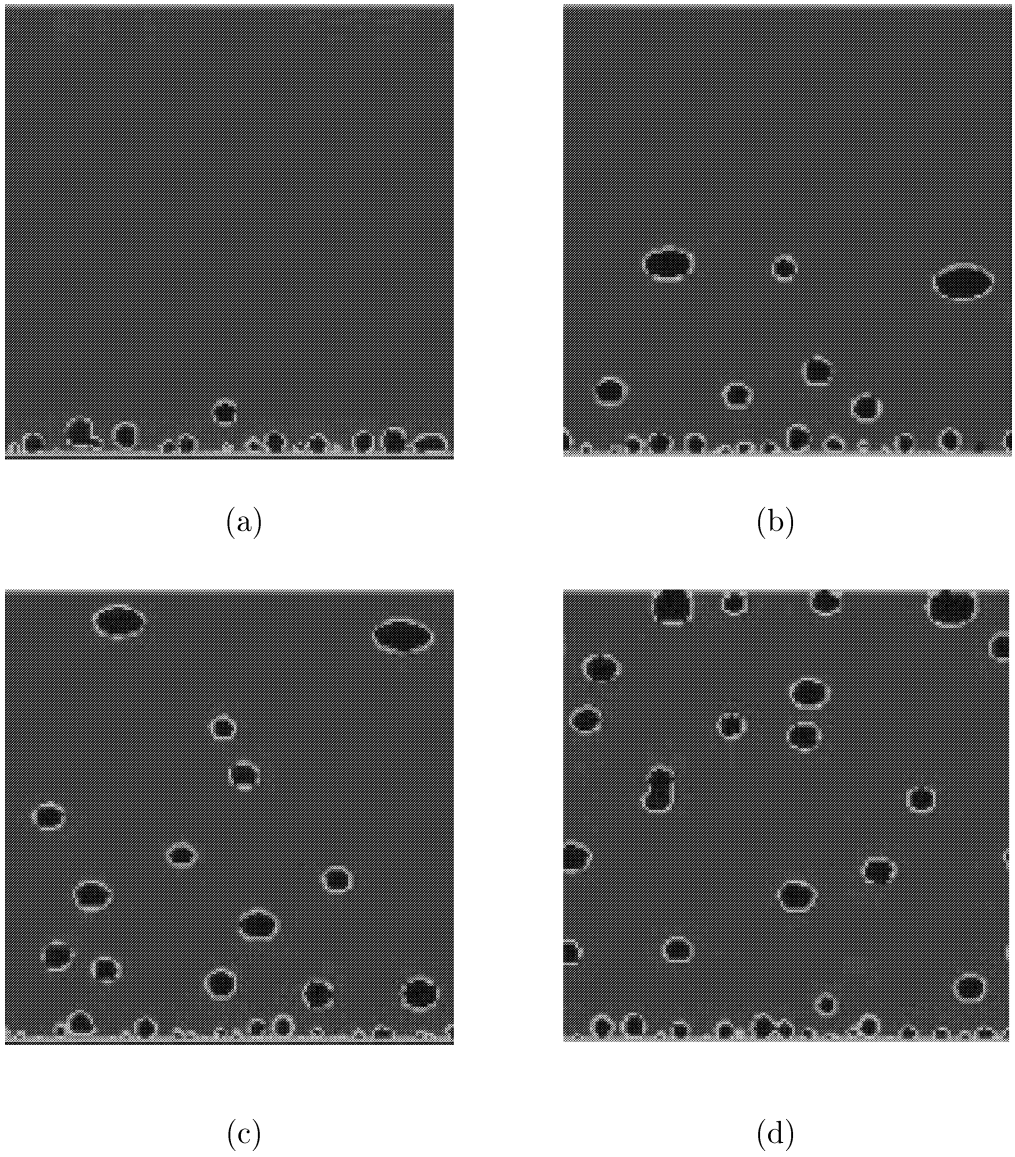

Fig. 3. Density distribution of pool boiling simulation with middle heat flux, $\Delta h = 0.01$. The gray color corresponds to vapor of lower density and black color corresponds to liquid of higher density. The times of figures (a), (b), (c), and (d) are 1000, 2000, 3000, and 4000 lattice unit, respectively.

and volume fraction. The simulations imitating pool boiling and boiling flow in a vertical pipe demonstrate qualitative applicability of the LB model to simulation of highly complicated multi-phase fluid phenomena. This LB model, however, have a intrinsic limitation that the energy conservation is not considered though the most realistic phase transitions are usually accompanied by heat evolution and absorption. In addition, treatment of large density variation and implementation of a realistic equation of state for water-vapor system still remain as future studies.

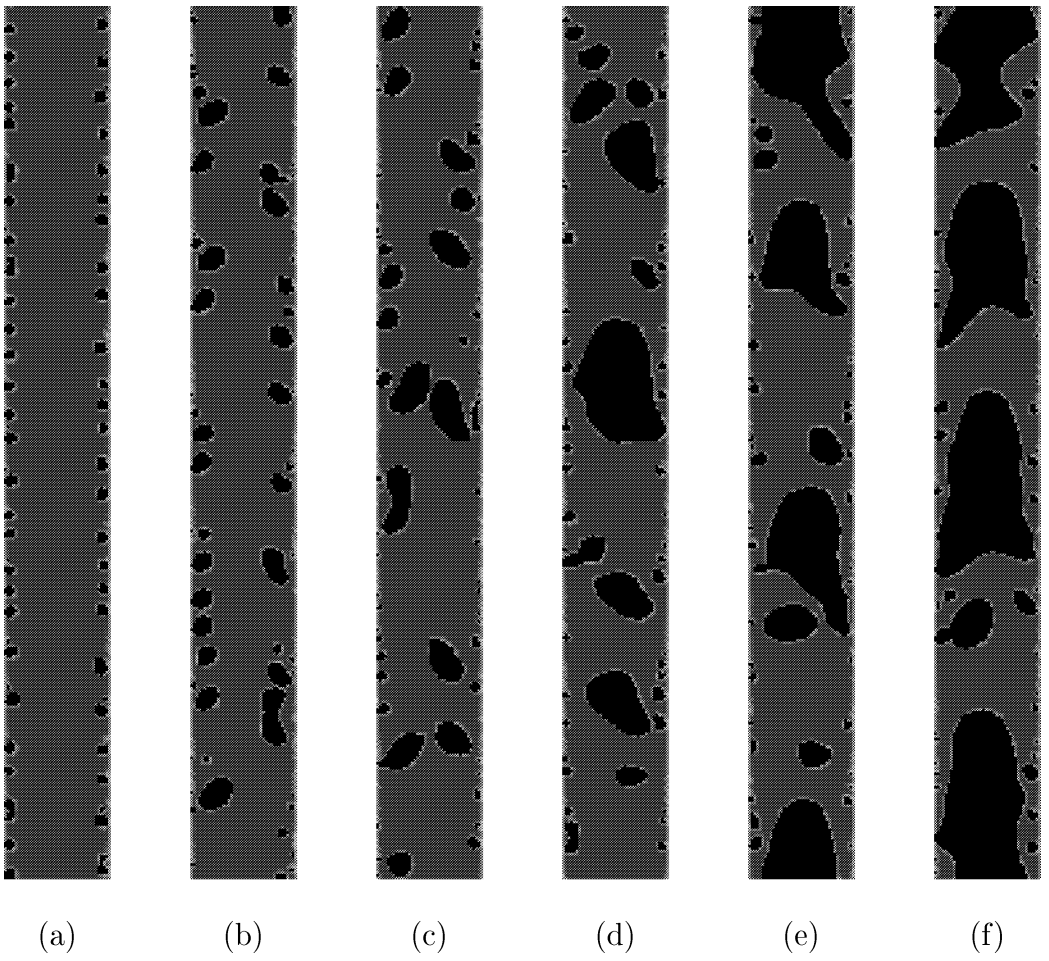

Fig. 4. Density distribution of boiling flow in a vertical pipe. The black color corresponds to vapor of lower density and gray color corresponds to liquid of higher density. The times of figures (a), (b), (c), (d), (e), and (f) are 100, 1000, 2000, 4000, 6000, 8000, and 10 000 (lattice unit), respectively. The flow pattern changes from liquid flow to bubbly and plug flow.

Acknowledgements

Authors are grateful to Prof. T. Ohashi of the University of Tokyo and Dr. S. Chen of Los Alamos National Laboratory for thoughtful and helpful comments. This work was supported by Ministry of International Trade and Industry, Japan.

References

[1] A. Tomiyama, A. Sou, H. Yoshikawa, T. Sakaguchi, J. JSME 60 (576) (1994) 2698.
[2] M. Sussman, P. Smerka, S. Osher, J. Comput. Phys. 114 (1994) 146.
[3] H. Takewaki, A. Nishiguchi, T. Yabe, J. Comput. Phys. 61 (1985) 261.
[4] U. Frisch, D. d'Humieres, B. Hasslacher, P. Lallemand, Y. Pomeau, J.-P. Rivet, Complex Systems 1 (1987) 649.
[5] S. Chen, H. Chen, D.O. Martínez, W.H. Matthaeus, Phys. Rev. Lett. 67 (1991) 3776.
[6] D.H. Rothman, S. Zalenski, Rev. Mod. Phys. 66 (1994) 1417.

[7] S. Chen, G.D. Doolen, Annu. Rev. Fluid Mech. 30 (1998) 329.
[8] A.K. Gunstensen, D.H. Rothman, Physica D 47 (1991) 47.
[9] D. Grunau, S. Chen, K. Eggert, Phys. Fluids A 5 (1993) 2557.
[10] X. Shan, H. Chen, Phys. Rev. E 47 (1993) 1815.
[11] Y.H. Qian, S. Chen, J. Modern Phys. C 8 (4) (1997) 763.
[12] M.R. Swift, W.R. Osborn, J.M. Yeomans, Phys. Rev. Lett. 75 (1995) 830.
[13] T. Seta, K. Kono, D.O. Martínez, S. Chen, J. JSME 65 (634) (1999) 1955.
[14] Y. Kato, K. Kono, T. Seta, S. Chen, D.O. Martínez, J. Modern Phys. C 8 (4) (1997) 843.
[15] F.J. Alexander, S. Chen, J.D. Sterling, Phys. Rev. E 47 (1993) 2249.
[16] Y.H. Qian, J. Sci. Comput. 8 (1993) 277.
[17] Y.H. Qian, P. Lallemand, Europhys. Lett. 17 (1992) 479.
[18] S. Chen, J. Wang, X. Shan, G. Doolen, J. Stat. Phys. 68 (1992) 379.